Back-vacuum Retarding Potential Analyzer for Investigation of Plasma Properties from Inertial Electrostatic Confinement Thruster

IEPC-2019-293

Presented at the 36th International Electric Propulsion Conference
University of Vienna • Vienna, Austria
September 15-20, 2019

Yung-An Chan[1] and Georg Herdrich[2]
University of Stuttgart, Stuttgart, Baden-Württemberg, 70569, Germany

A prototype of a back-vacuum retarding potential analyzer (RPA) is proposed, developed and set-up to resolve a known issue occurring in the conventional RPA measurement: particle accumulation. In doing so the relevant design parameters are presented combined with a strategical evaluation for this innovative design concept. The evaluation reveals significant improvement on maximum ion flux density which is up to 10^{18} m^{-3} (conservative value) according to the analyses. This provides a reliable and accurate measurement basis for high density electric propulsion device/plasma source in the future which is in turn the prerequisite for the determination of ion and electron energies and corresponding verifications such as the determination of thrust.

Nomenclature

ε_0	=	vacuum permittivity
δ	=	grid transparency
λ_D	=	Debye length
D_a	=	probing aperture of RPA
d_c	=	characteristic length of grid's cell
e	=	electron charge
k_B	=	Boltzmann constant
n_e	=	electron density
T_e	=	electron temperature
t_s	=	plasma sheath thickness
V_g	=	grid biased voltage
w_c	=	characteristic distance between cells on the grid
C	=	collector
EB	=	electron beam
ERG	=	electron retarding grid
ESG	=	electron suppression grid
FP	=	Faraday probe
FG	=	floating grid
IEC	=	inertial electrostatic confinement
IEDF	=	ion energy distribution function
IRG	=	ion retarding grid
IRS	=	Institut für Raumfahrtsysteme (Institute for Space Systems)

[1] PhD candidate/Research associate, Institute of Space Systems, chan@irs.uni-stuttgart.de
[2] Head of plasma wind tunnels and electric propulsion, Institute of Space Systems, herdrich@irs.uni-stuttgart.de

l_{gap}	=	gap length between ERG and IRG
RPA	=	retarding potential analyzer

I.Introduction

Development of inertial electrostatic confinement (IEC) device at IRS has become concrete and mature since 2017.[1] Advanced plasma source concepts and space propulsion designs based on the extracted plasma are proposed and summarized at the IEPC 2017 and the IAC 2018, respectively.[1,2] More detail regarding to the extracted electron beam, as known as tight jet, has been revealed, which helps in the estimation of plasma properties in the core and supports the design of the IEC plasma source. [3] However, the knowledge with respect to the spray jet mode is still limited. To fully understand the plume characteristic of an IEC for further application as electric propulsion, relevant plasma diagnostics for the spray jet is required.

Based on the preliminary measurement from Faraday probe (FP), the spray jet is very different from the electron beam (EB) extraction in tight jet condition - it is rather like a low temperature quasi-neutral plasma plume instead of a jet almost purely dominated by electrons. Figure 1 shows the case comparison of FP measurement in tight jet as well as spray jet plume at 30 cm away from the extraction port of the opened grid IEC, which shown in previous investigation.[3] The measurement of tight jet (red marks) indicates an upward shifted current-to-voltage curve (much higher positive current in a negative biased probe). This is due to secondary electron emission on the collector surface induced by high-energy EB bombardment. This interpretation is verified in Ref. 3. The electron saturation density and electron temperature from both jet condition can be identified with Ref. 4. The measured electron density is in the range of 10^{14} m^{-3},this is due to the open grid structure of the used laboratory IEC, which causes the plasma diffusing openly to the vacuum. It is expected to be much higher in a closed IEC plasma source.[5]

The measurement result in spray jet (blue marks) has floating potential at -0.1463 V which suggests that the plasma is extremely close to quasi-neutrality though electrons are slightly more than ions at this measured position. Two possible items might cause this quasi-neutrality. First, the spray jet is generated by a low population of high-energy diffused electron plume extracted from the core of the IEC (but still much lower than tight jet due to lower applied voltage on the cathode). These induce electron-impact ionization with the heavy particles on the way out and provide a significant amount of secondary electrons and ions on the plume trajectory. Accordingly, it is majorly composed by the low temperature secondary ions and electrons.

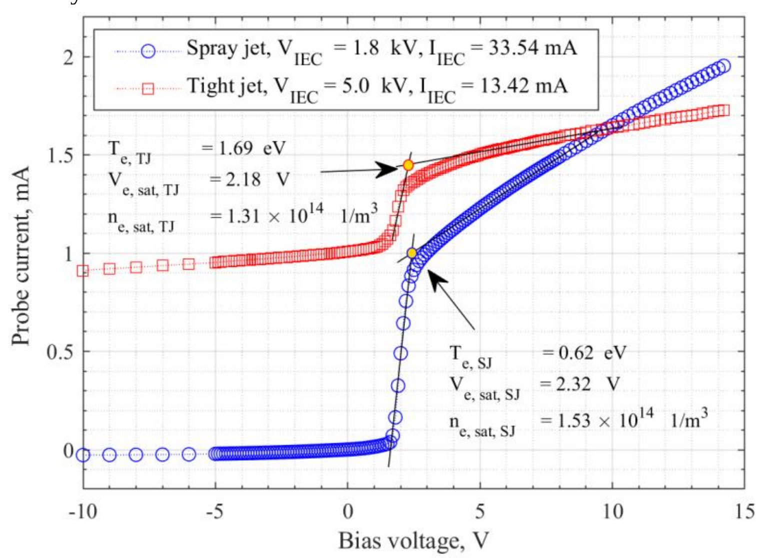

Figure 1   Comparison of Faraday probe measurement in tight jet and spray jet with plasma properties

However, it might be tricky to identify small population of electron with moderate kinetic energy in a highly populated low temperature electron because the signal might be concealed by the ion saturation current. Figure 2 shows the same result at large negative biased voltage. The measured current from the tight jet remains in the positive with -200 V on probe due to the intensive secondary electron emission on probe surface. This provides a large contrast to the "classical" ion saturation current. On the other hand, the probed current in spray jet are around the same order of magnitude as ion saturation current, which increases the difficulty to identify the dominance of measured current from the other.

The second possible item could be that the quasi-neutral plasma is directly coming from the core of the IEC which extracts about the same number of ions and electrons. If this is true, the ions should have higher kinetic energy to escape the negatively biased potential on the IEC cathode. A retarding potential analyzer (RPA) can resolve which of the two scenarios described here are relevant.

An RPA is a powerful plasma diagnostic tool, which determines the kinetic energy of the charged particles (possibly the densities as well) for the plasma plume.[6] The basic concept of an RPA is composed by a set of metal grids, each of them is biased with different voltages for repelling charge particles. However, the conventional RPA has a limitation in testing high density plasma sources [6,7], a feature that is likely also the case for the plume of the IEC spray jet. To solve this issue, a back-vacuum RPA has been developed at IRS.

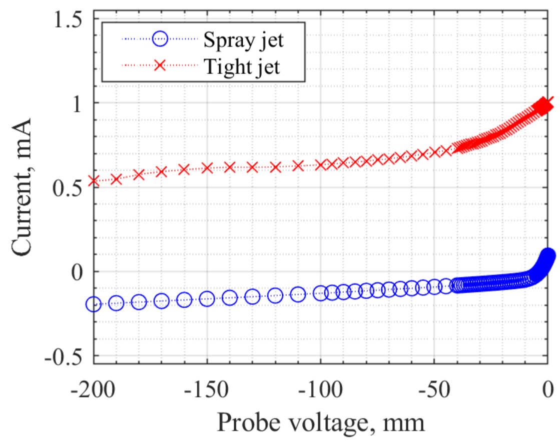

Figure 2 Comparison of FP measurement in tight jet and spray jet at high negative biased voltage

The advantage of back-vacuum RPA is the special design of the grid pack, which prevents the accumulation of heavy particle density within the packed grid. A pumping mechanism is connected to the probe to remain a certain vacuum degree (or pressure level) and to reduce the scattering effect from particle collisions. Second, the grid is manufactured by an advanced manufacturing processes called laser-micro-drilling, which enables much lower cost and remains respectively high accuracy compared to the usual lithography processes. Apart from this, the restriction on the material selection for grids are much less, which make the use of materials with high thermal resistance and lower electron emission be possible. These can potentially improve the accuracy of the measurement result from traditional RPA concept.

In this paper, the design principle of the back-vacuum RPA will be introduced. The evaluation of the design parameters is presented and the design criteria for the pressure release mechanism are described. Secondly, the manufacture methods and concerns for the grid will be summarized in this paper as well. The experimental setup and arrangement will be presented to summarize the test preparation status for IEC thruster characterization in the future.

II.RPA designs

A. Conventional RPA design

Figure 3 shows a schematic of a 4-grid RPA, each of them serves for a different purpose. The floating grid (FG) is the first one that is confronted by the plasma plume. In order to mitigate a perturbation of the given plasma properties, the grid remains floated to the plasma. The electron retarding grid (ERG) is biased to negative potential to repeal all the electrons that pass through the FG and only allows ions to pass to the next grid. The ion retarding grid (IRG) is applied with positive potential, which serves as a high-pass ion energy filter. This grid usually sweeps around to adjust and determine the kinetic energy threshold. The ions that are able to pass through the potential barrier will reach to the collector; while the others will be repelled and remain in between ERG and IRG. Ions that collide with collector (C) will be neutralized by the slightly negatively biased collector. The ion bombardment might create the secondary electron emission from the surface of C and distorted the measured result. Thus, an electron suppressing grid (ESG) is implemented between IRG and C to repel the secondary electron emission back to the it surface. By analyzing the

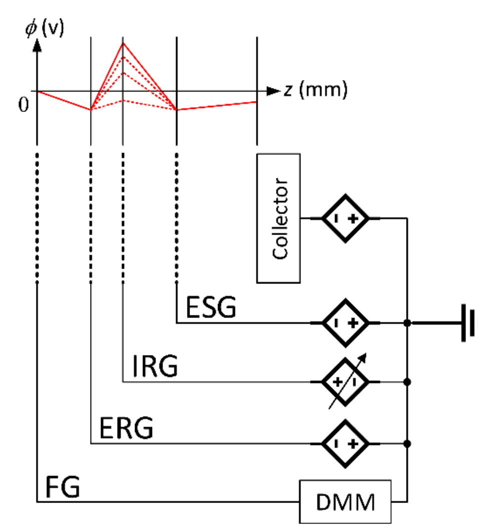

Figure 3 Schematic concept of conventional RPA

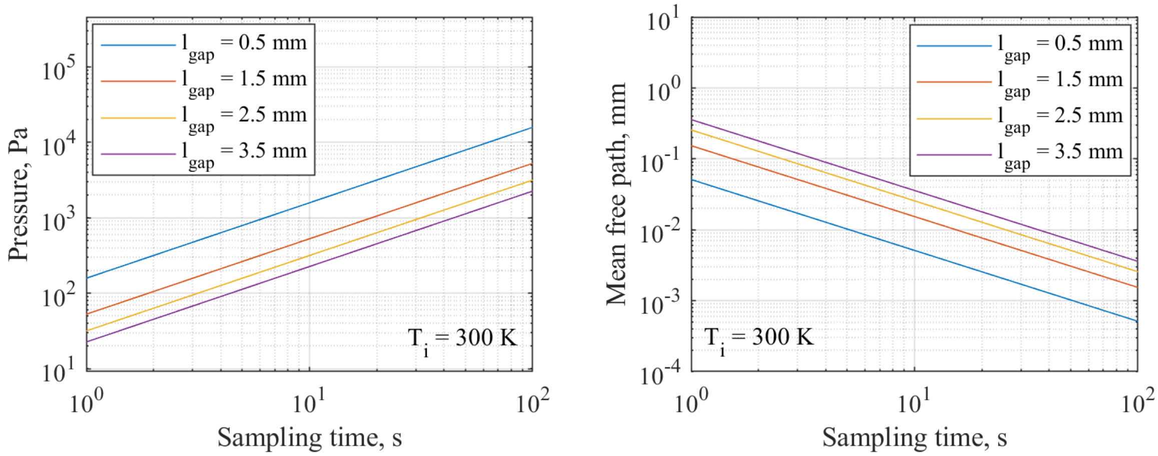

Figure 4 Rough estimation of pressure and mean free path respect to the sampling time inbetween a pair of infinity large grids with a finte grid distance, assuming influx ion density at 10^{15} m^{-3} and kinetic energy 300 eV

correlation of collector's measured current and the biased voltage on the IRG, the ion energy distribution function (IEDF) is revealed.

Althought RPA is powerful for measuring the IEDF, several issues influence the accuracy of measurement result as well as the reliability of the probe. First of all, the plasma properties are varied greatly from plasma source to plasma source. It is difficult to have a single RPA to cover all different kinds of plasma source. Second, the accumulation of the charged particles brings up the pressure within RPA, especially in between ERG and IRG. [6–8] This causes a scattering of the ion trajectory, ion energy broadening, as well as the charge-exchange effect, which degrades the accuracy of measurement. The worst is the electrical breakdown due to high differential voltages between the grids in a high-pressure environment. [7] Assuming an infinite incoming area with all the incoming ions repelled by IRG and trapped, the pressure in certain gap length (l_{gap}) to the measuring time can be calculated. The ion density and kinetic energy is assumed with 10^{15} m^{-3} and 300 eV, respectively. Figure 4 is a rough estimation of pressure raising in-between IRG and ERG with certain amount of ion influx. The pressure in the gap between IRG and ERG increase significantly fast. The mean-free-path of the particle, charged or non-charged, are becoming smaller than the grid after few second of sampling, in which the particles possibly pass through the grid gated. Although this could be eased by reducing ion influx via decreasing the grid transparency, the signal-to-noise ratio might become too small for reliable analysis. Moreover, particles will eventually accumulate in the volume and build up the pressure if the measuring time is taken too long. This is especially critical for characterization of high-density plasma. Last, it is possible to perform a short sampling time and block the plasma influx to RPA. This could allow the accumulated particle diffusively released through the grids. But it would massively increase the testing time for a single measurement. This suggests the design of a particle releasing mechanism is mandatory.

B. Evaluation of grid and spacing parameters

1. Sheath thickness and cell size

Sheath thickness is the most important parameter for RPA design, which is correlated to the (local) Debye length of the plasma. Both parameters are shown in following Eq. 1 and Eq. 2. [6,7,9]

$$\lambda_D = \sqrt{\frac{\varepsilon_0 k_B T_e}{e^2 n_e}} \qquad \text{Eq. 1}$$

$$t_s = 1.02\lambda_D \left(\frac{eV_g}{k_B T_e}\right)^{3/4} \qquad \text{Eq. 2}$$

Here, ε_0 is the vacuum permittivity, k_B and T_e are Boltzmann constant and electron temperature, e is the electron charge, and n_e is the electron density. The size V_g is the biased voltage on the grid.

According to references [6,7,9,10], the grid size should be at least smaller than the sheath thickness to avoid the distortion of electric field on the grid opening, which causes electron leak through the cells to the other size. The

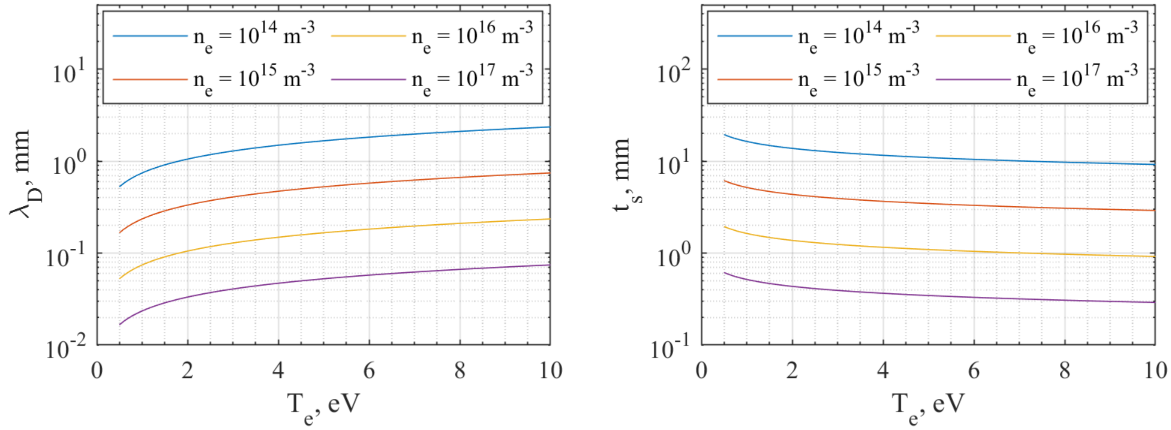

Figure 5 Calculation of Debye length and sheath thickness to the electron temperature at different electron density

thickness of sheath scale is usually in the range of 2 – 10 times of Debye length of the measured plasma, depending on the grid voltage. [6, 9,11] Both parameters correlate to the electron temperature as well as electron density for the incoming plasma are shown in Figure 5. This provides the basic information for the design of gird's cell dimension and the grid spacing.

2. Grid pattern

The grid pattern determines the transparency of the grid and accordingly the amount of incoming plasma and the signal-to-noise ratio for the current. Three parameters are related to the grid pattern: shape, cell size, and cell distance. Figure 6 defines the characteristic dimension respect to the cell shape applied.

The characteristic size is defined as the length of the cell's edge (d_c), which is correlated to λ_D determined in previous subsection. The characteristic distance (w_c) indicates the distance between cells, which is usually ignored in the conventional RPA design. However, the size of w_c has the same effect as the size of cell regarding to the uniformity of the electric field. If w_c is too small, it is not possible to generate a flat equal-potential line which is parallel to the surface of the grid. Non-uniform electric potential gradients will cause an electrostatic lens effect for the incoming

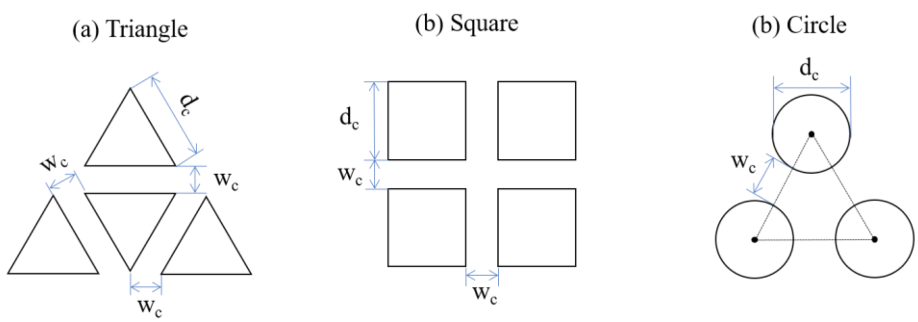

Figure 6 Illustration of cell's shape for grid pattern and their characteristic dimensions

plasma and allow more ions going through the cells. In order to generate a uniform equal-potential line on nearby grid, it should be also larger than the sheath length as well.

The ratio between these two characteristic dimensions summarizes the correlation of cell size and their distance, which is formulated by w_c/d_c. If the ratio gets smaller, the cell's area becomes larger which improves the transparency of the grid but reduces the electric field uniformity, and vice versa. To achieve a certain transparency and uniformity of the electric field, the ratio is set to one in this prototype for further evaluation.

The estimation of total cell's number and the grid's transparency for the three different cell shapes are shown in Figure 7. The aperture for plasma collection in the RPA is assumed with ϕ12 mm. The cells are assumed uniformly distributed within the region of the aperture. It is clear that the square cells provide the highest transparency for the grid compared to the triangular and circular shape, no matter which d_c is selected for the cell size. Therefore, the square shape is selected for the RPA grid pattern.

3. Grid spacing

Based on the Child-Langmuir theory, the space between the IRG and ERG should be smaller than the sheath's dimension in order to avoid space-charge limitation. [6, 9,12,13] This happens when too many charges are accumulated in the space between IRG and ERG, which produces higher space potential than the bias voltage on IRG. This creates a potential barrier that hinders further ions from passing (through this space). Two solutions can mitigate this issue: The first one is to decrease the incoming flux of ions to further increase the Debye length. The second solution is to minimize ion moving to transverse direction of the grid by a decrease of the distance between both grids below the sheath thickness. [6]

The second measure could potentially reduce the number of particles accumulated in between IRG and ERG by limited their transverse motion, but this will eventually accumulate some charge particles due to slight misalignment of grids or repelling force applied on the charge particle. In addition, maintaining a smaller gap distance for the two grids becomes more difficult at very low distances (say below 0.5 mm). [6] This restricts the RPA's capability in plasma density below 10^{16} m^{-3} (e.g. see Figure 5.). Furthermore, according to Figure 4, the increase of the pressure slope is too fast to perform a reliable measurement when the distance between the grids is too low. This measure should be considered together with the pressure release mechanism. To effectively release the accumulation of particles, the design of the releasing area should be equal or larger than the total transparent area on the grid.

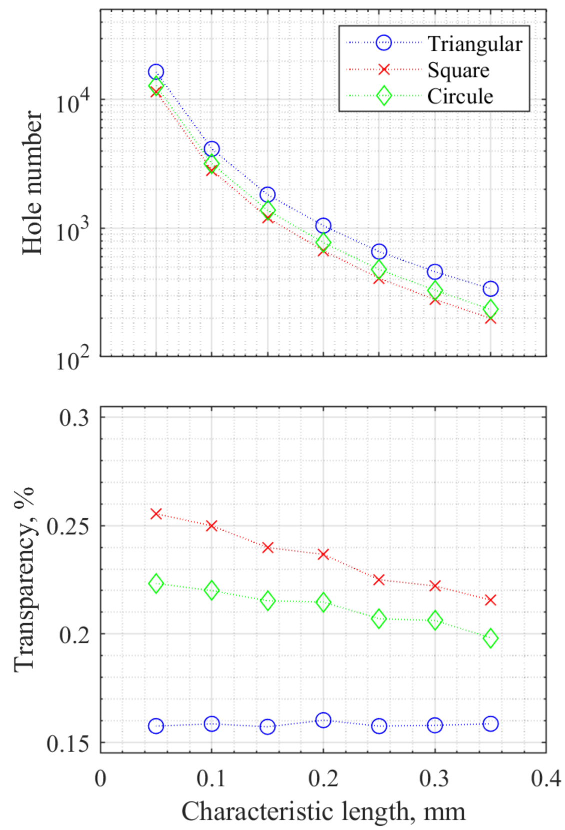

Figure 7 Calculation of acceptable number of cell and transparency in different cell's shape on a distributed on a ϕ12 mm aperture.

4. Grid thickness and tilt angle on the cell's wall

The influence of grid thickness and tilt angle between each cell's wall to the grid surface is rarely discussed in literature. Based on simulation results in Ref. 14, the grid with finite thickness indeed has smaller incoming current flux than ideal zero-thickness grid. In addition, larger tilt angle also enhances the collecting current. This is probably a result from the electrostatic lens effect formed by the cell's aperture and wall. However, the currently the authors do not find more detail experimental discussion on the comparison of these two parameters with respect to the resulting

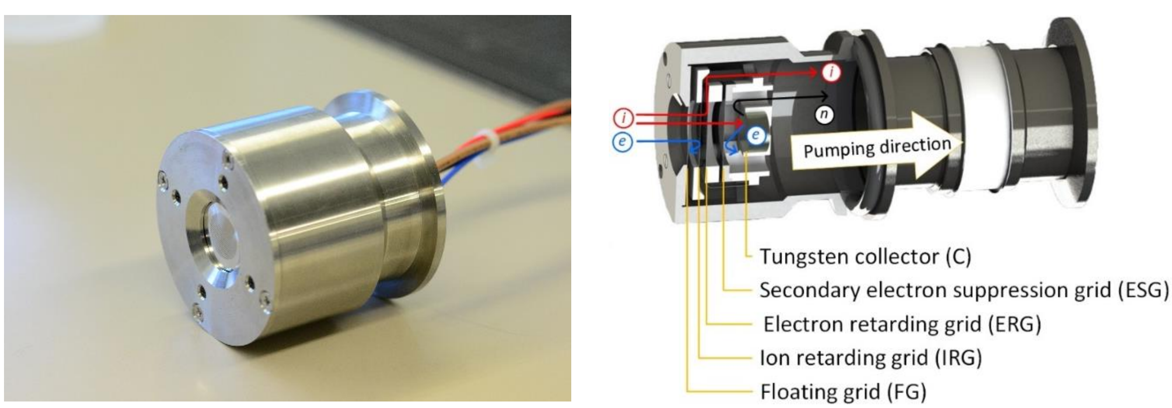

Figure 8 Picture of back-vacuum RPA and CAD cross-section of grid pack arrangement

RPA properties. Accordingly, the thickness is set at 50 μm, which is smaller than the characteristic length of each cell, while the tilt angle is zero degree.

C. Prototype of back-vacuum RPA

Figure 8 shows the detail of the IRS back-vacuum RPA, which is a four-grid system. The design of an opened grid-pack assembly allows the accumulated particles to be released from the transverse direction of grids. In between ERG and IRG, a reflection wall is implemented right at the exit to mitigate the backflow of the released heavy particles. The back of the RPA is designed as an KF40 flange serving as interface for a turbopump to be attached. This is to pump out the continuous particle influx and hence to stabilize the pressure in RPA grid set. The design parameters are summarized in the following Table 1.

Table 1. Summary of design parameters for back-vacuum RPA

Parameters	Dimension	Unit
RPA body		
Aperture (D_a)	12	mm
Outer diameter	54	mm
Body length	51.5	mm
Grid		
Material	SS 316	
Aperture	12	mm
Transparency (δ)	24.99	%
Cell shape	square	
Cell size (d_c)	100	μm
Cell distance (w_c)	100	μm
Cell thickness	50	μm
Spacing & Insulation		
Material	MACRO/Alumina (99.6 %)	
Grid distance (FG to ERG)	3.55	mm
Grid distance (ERG to IRG)	1	mm
Grid distance (IRG to ESG)	5	mm
Grid distance (ESG to C)	6	mm
Collector		
Material	Tungsten (99.5 %)	
Collecting area	12	mm

The cell size of the grid is determined based on the evaluation of sheath thickness (see above and see Figure 5.), which allows to perform reliable measurements for plasma densities of more than 10^{17} m^{-3} (possibly up to 10^{18} m^{-3} depending on the transparency of the grid). The space between ERG and IRG is determined based on the transparent area on the grid, which is summarized in Eq. 3. Therefore, l_{gap} = 1 mm is selected in this prototype.

$$l_{gap} \geq \left(\frac{\pi {D_a}^2}{4} \times \delta\right) / \pi D_a \geq \frac{\delta D_a}{4} \qquad \text{Eq. 3}$$

The insulation between the grids is composed by MACOR due to its machinable characteristic and alumina washers for its accessibility and lower price. Tungsten is chosen as the material for the collector because of its low secondary electron emission rate from ion bombardment.

The performance of back-vacuum RPA is evaluated with the steady pressure in between the ERG and IRG with the probe design parameter. Assuming all the ion flux pass through the ERG are decelerated in a finite gap distance by the fully retarding potential without encountering charge-exchange effect, the balance condition of incoming ion flux and release ion flux can reach to a steady pressure. Accordingly, pressure can be calculated with known ion influx density, kinetic energy, and temperature. Hence, their respective mean free path as well as the sheath thickness can be evaluated with the design parameter of back vacuum RPA. Figure 9 shows the estimation of ion influx density to finite gap distance between ERG and IRG in the assumption of ion kinetic energy 600 eV and ion temperature of 1eV. The probe geometry can be found in Table 1 above. The mean free paths, indicating the probability of scattering by ion-

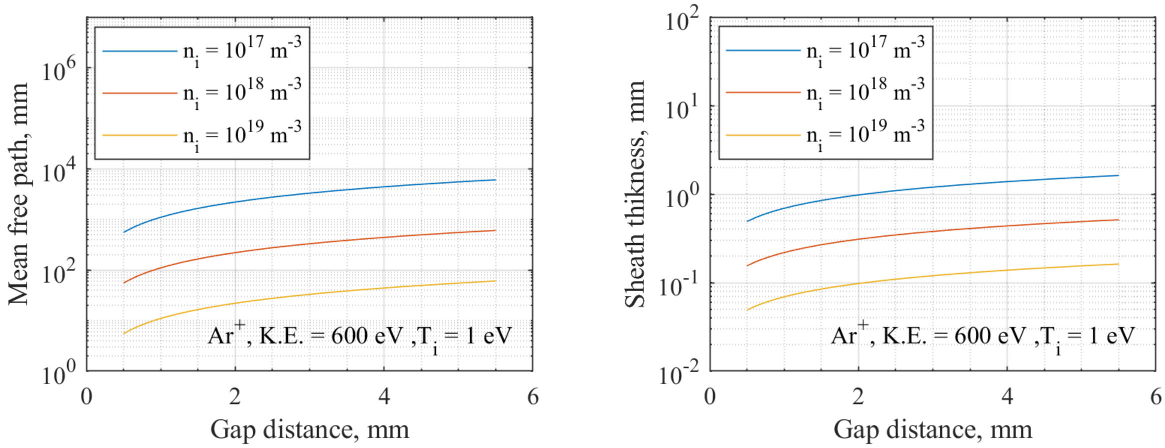

Figure 9 Evaluation of mean free path and sheath thickness in a finite gap distance with assumption of Ar^+ in kinetic energy (K.E.) 600 eV, T_i = 1 eV.

ion collision in the respective pressure balance condition, are low; while the sheath thickness suggests the accumulated particles are unable to leak through the IRG with the designed cell dimension in case of ion influx density at 10^{18} m^{-3}. The results demonstrate that the back-vacuum RPA could greatly improve the capability of testable ion density envelopes up to 10^{18} to 10^{19} m^{-3}. This proves that the design can greatly improve the reliability of measurement result as well as prevent the electrical breakdown when operating in high voltage.

The electrical circuit is composed by three difference sourcemeters, respectively. The ERG and ESG are connected to same power supply (Aim-TTI PHL120), which is capable to supply voltage up to -120V. The IRG is connected with Keithley 2410, which has the capability for the wide voltage sweeping (from 0 to 1100V) with extremely high voltage precision. The collector is connected with Keithley 2450 which provides extremely high accuracy on current reading. The FG and outer case of RPA will be kept in floating to the plasma and connected to a digital multimeter to measurement the floating potential. An independent turbopump with fore-vacuum is connected though a flexible metal hose to the back of the RPA. To remain floating voltage on probe body, an insulator with KF40 flange is connected between the RPA and hose.

A. Manufacturing Process for the Grids

Figure 10 shows the manufactured grid for back-vacuum RPA, which is manufactured by laser-micro-drilling. The concept of this technology uses pico-second laser pulses to provide very precise and distinct ablation at the specific position. [15] The sharpness of the cell's edge is determined by the size of laser focal point [15,16], pulse repetition, and pulse energy. [17,18] The precision of the beam position and maximum depth of the drilling material depends on the beam motion optics. The precision of positioning can go down to 62.64 nm, while the maximum thickness of the material can reach to 2 mm nowadays and still remain high accuracy and edge sharpness. [19] It not only provides fast and precise production for a lot of sharp-edge holes which is extremely beneficial to 2D pattern, but also minimizes thermal impact

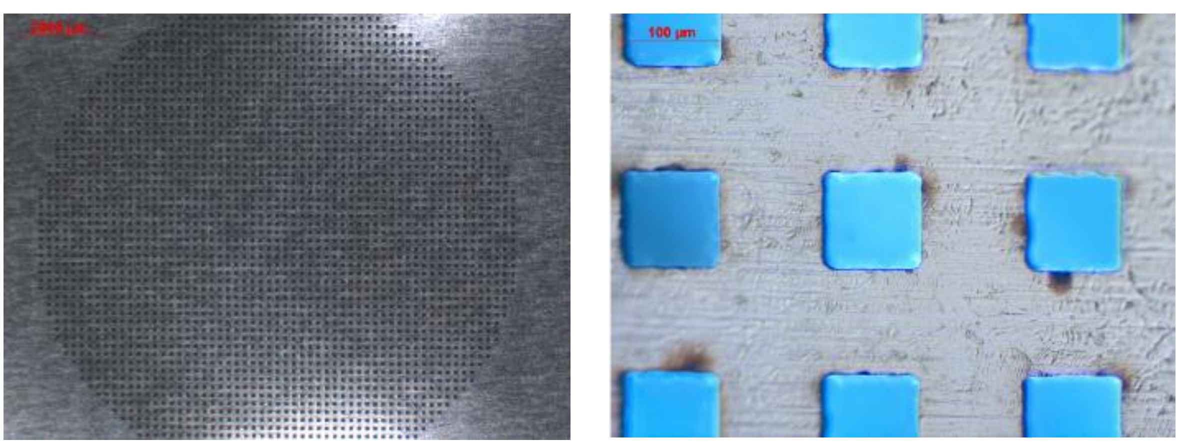

Figure 10 RPA grid pattern which is manufactured by laser-micro-drilling processes

to the surrounding material. [20,21] The processes do not require special pre-treatment or post-treatment. In addition, it is flexible to the selection of drilling materials and can flood with inert gas to further avoid oxidation when processing in the ambience. The parameters for the manufacture of the grid is listed in the following Table 2.

Table 2. Parameters and setup for RPA grid manufacture

Parameters	Setup/Value	Unit
Laser type	Lumentum Duetto	
Beam motion optics	Scanlab - Hurryscan II 14	
Laser wavelength	1064	nm
Focal diameter	20	µm
Pulse energy	30	µJ
Pulse duration	8	ps
Repetition rate	10	kHz

III.Test with IEC plasma source

B. IRS Tank 12 facility

Tests for IEC plasma source and plasma diagnostics are performed in the IRS Tank 12 facility, which is depicted schematically in Figure 11. A ϕ1 m * 2.75 m vacuum chamber with a three-stages pumping system offers maximum pumping capability up to 2400 m^3/hr with nitrogen and a base pressure down to 0.05 Pa.

The IEC power supply is an electron source (HVPS), which provides up to -20kV with 10 kW maximum power output. The flow-control-unit (FCU) has two thermal mass-flow-controllers to provide precise gas supply down to 50 $\mu g/s$ with argon. All signals are connected and recorded via data-acquisition system (DAQ). A digital camera (DSLR) is monitoring the thruster operation and discharge channel from the window on the tank.

A three-dimensional closed-loop-controlled platform is implemented in the vacuum tank. It could provide two translational and one rotation motion with control precision down to 0.1 mm and 0.5°, respectively. This offers precise positioning for plasma diagnostic tools and enables spatial characterization for plasma plume. The detail specification of the platform can be found in the following **Table 1**Table 3. The RPA and other diagnostic tools will be mount on the platform to perform spatial characterization for IEC plume.

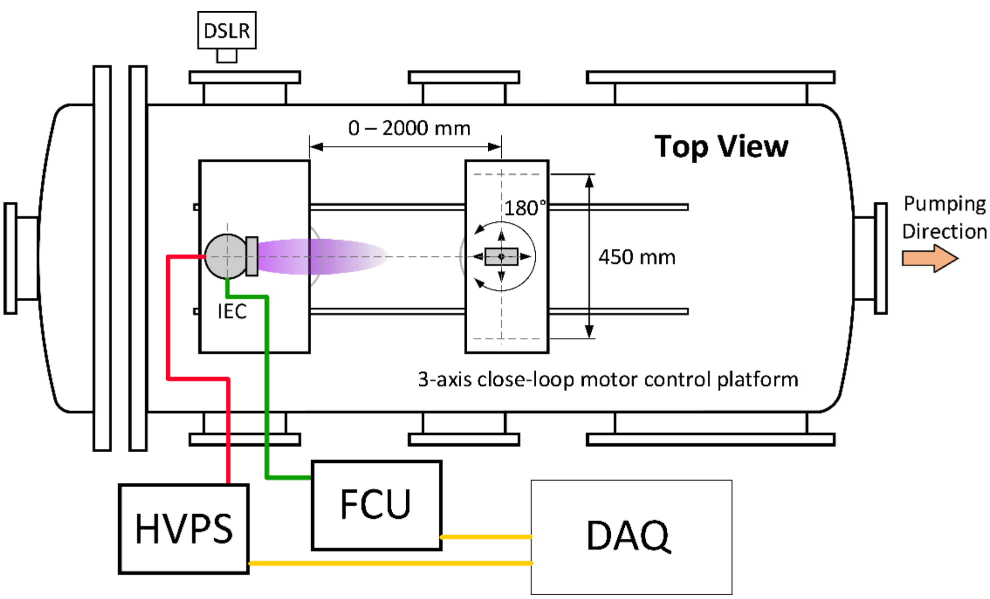

Figure 11 Overview of Tank 12 test facility's interface and arrangement

Table 3 Specification of 3-axis close-loop motor-controlled platform

Function	Specification	Unit
Motion Coordinator	Raspberry Pi 3	
Axis control frequency	100	Hz
No. of axis	3 (planning for 4)	
Command/Readout	Labview®	
X translation		
Stroke	Up to 2000	mm
Pos. Precision	0.025 (stepper motor) + 0.07 (screw)	mm
Pos. Accuracy	0.005	mm
Max. speed	93.75 (estimated without load)	mm/s
Y translation		
Stroke	400	mm
Pos. Precision	0.01 (stepper motor) + 0.07 (screw)	mm
Pos. Accuracy	0.002	mm
Max. speed	37.5 (estimated without load)	mm/s
Z Rotation		
Degree	180	degree
Degree Precision	0.36 (stepper motor) + 0.133 (gear)	degree
Degree Accuracy	0.205 (estimated)	degree
Max. speed	80 (estimated without load)	rpm
Communication IF		
Ethernet	For commending and position readout	
BNC * 4	For synchronization (up to 1 MHz)	
Sub-D9 * 4	Digital I/O (up to 1 MHz)	

C. IRS IEC plasma source

The IEC plasma source for plume investigation is shown in Figure 12. [2,5] The spherical hollow anode has an inner diameter of 147 mm with a 3D-printed cathode grid. The cathode grid is designed based on the truncated cuboctahedron pattern with refine vertices and plasma extraction port. The goal is to achieve good confinement of plasma by the super-symmetrical grid arrangement as well as to provide electric potential gradients to enable extraction of plasma.

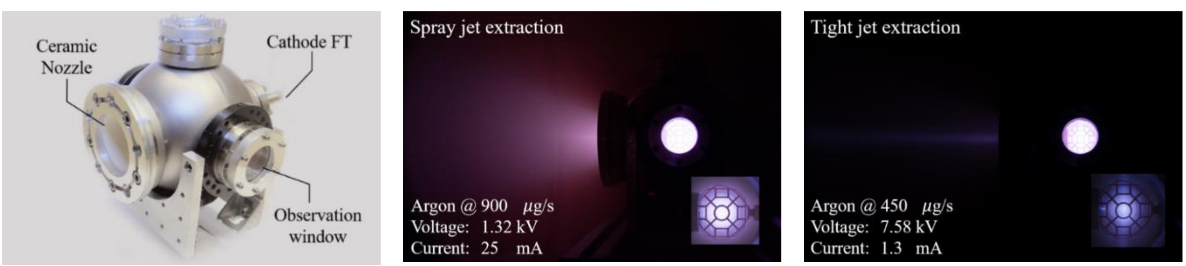

Figure 12 Assembly of IEC plasma source for RPA measurement (left), operation of IEC plasma source in spray jet mode (middle), and tight jet mode (right)[5]

Four CF40 ports are implemented on the equator plane of the hollow anode, of which the axes are 90-degree to each other. They are design for the observation of discharge behavior or for non-invasive plasma diagnostics. In addition, an extra CF40 flange and a CF75 port are center-aligned and placed respect to the zenith and nadir of the anode, which serves and the power feeding port and plasm extraction port respectively. The ceramic nozzle, attached between the extraction port and cathode, provides enclosure of the discharge chamber and electrical insulation. A special design on the insulation of cathode feedthrough prevents the electrical breakdown from the high differential voltage between power feeding line to the anode (up to 10 kV). More detail regarding to the IEC plasma source design and discharge behavior can be found in Ref. 5.

IV. Conclusion

The RPA is a powerful plasma diagnostic tool, which is capable to provide kinetic energy distribution function of ion species. However, conventional RPAs suffer from the issue of particle accumulation in between ERG and IRG during measurement, which cause ion scattering and leads to the broadening of kinetic energy spectrum. If the number of accumulated particles is too high, the gap in-between ERG and IRG might reach to the space charge limit or induces electrical breakdown (arcing). This issue might be able to be resolved by minimizing the transverse motion of particles within the grid pack, e.g. reduction of gap distance to a value smaller than the sheath thickness with perfectly aligned grid pack. However, regarding a realistic sampling time and the mechanical tolerance, it is not able to perform reliable measurement in high density plasma. Accordingly, a back-vacuum RPA is designed to overcome this restriction.

The concept for back-vacuum RPA is simply provide a release mechanism for accumulated particles within grid pack on the transverse direction of the grid. The cell dimension is designed to provide uniform retarding field with maximum transparency to reduce the electrostatic lens effect occurred on the incoming particle and remain signal-to-noise ratio. The lower limit of the gap distance could be decided by calculating the grid's transparent area and its peripheral length; while the upper limit is determined by the calculated sheath thickness. The released particles are diffused away from the grid pack and removed from the probe by a turbopump. This allows back-vacuum RPA to perform continuous measurement for high density plasma.

The back-vacuum RPA presented in this paper are capable to perform reliable measurement continuously for plasma density up to $10^{18}\,m^{-3}$ (conservatively speaking). The electrical circuit enables sweeping voltages of up to 1100V with very high precision on the current sensing. It offers a very sustainable basis for characterizing the plasma plume from high density electric propulsion/plasma source.

The plasma characteristics from an opened grid IEC was briefly characterized. The low ion saturation current density suggests the ion density are quite low in this configuration. This is due to the open-grid configuration which allows the extracted ions diffused into free space. Enhancement of ion current density is expected in the enclosed IEC plasma source. Furthermore, the under-developing electromagnetic nozzle for plasma collimation and acceleration could provide more dense plasma plume. Back-vacuum RPA is designed for this purpose and is an ideal tool for the verification of IEC plasma properties in the near future.

V.OUTLOOK

The plan in the near future is to perform the spatial-resolved plume measurement for the IEC plasma source with Langmuir probe as well as Faraday probe developed in IRS. This can provide the first understanding on the plume characteristics, e.g. T_e, n_e, and divergence angle, to determine the measurement strategies for RPA (test case, sampling time, and probing position, etc.).

Acknowledgments

The author would like to express his gratitude to Dr. Christian Freitag from LightPulse GmbH for the support on the knowledge basis of laser micro drilling as well as manufacture of the metal grid.

References

[1] Chan, Y.-A., and Herdrich, G., "Inertial Electrostatic Confinement: Innovation for Electric Propulsion and Plasma Systems," *35th International Electric Propulsion Conference*, IEPC 2017-599, Atlanta, GA, U.S.A, 2017.

[2] Chan, Y., and Herdrich, G., "Breakthrough of Inertial Electrostatic Confinement Concept for Advanced Space Propulsion Y.-A. Chan," *69th International Astronautical Congress*, IAC-18,C4,7-C3.5,12,x47993, Bremen, Germany, 2018, pp. 1–5.

[3] Chan, Y.-A., and Herdrich, G., "Jet extraction and characterization in an inertial electrostatic confinement device," *Vacuum*, vol. 167, Sep. 2019, pp. 482–489.

[4] Chen, F. F., "Lecture Notes on Langmuir Probe Diagnostics," *IEEE-ICOPS meeting*, 2003, pp. 1–40.

[5] Chan, Y.-A., and Herdrich, G., "Influence of Cathode Dimension on Discharge Characteristics of Inertial Electrostatic Confinement Plasma Thruster," *36th International Electric Propulsion Conference*, IEPC-2019-292, Vienna, 2019.

[6] Hutchinson, I. H., *Principles of Plasma Diagnostics*, Cambridge University Press, Cambridge, 2002.

[7] Zhang, Z., Tang, H., Zhang, Z., Wang, J., and Cao, S., “A retarding potential analyzer design for keV-level ion thruster beams,” *Review of Scientific Instruments*, vol. 87, Dec. 2016.

[8] Denieffe, K., Mahony, C. M. O., Maguire, P. D., Gahan, D., and Hopkins, M. B., “Retarding field energy analyser ion current calibration and transmission,” *Journal of Physics D: Applied Physics*, vol. 44, Feb. 2011.

[9] Azziz, Y., “Experimental and theoretical characterization of a Hall thruster plume,” 2007.

[10] Böhm, C., and Perrin, J., “Retarding-field analyzer for measurements of ion energy distributions and secondary electron emission coefficients in low-pressure radio frequency discharges,” *Review of Scientific Instruments*, vol. 64, Jan. 1993, pp. 31–44.

[11] Zhang, Z., Tang, H., Zhang, Z., Wang, J., Cao, S., Zhang, Z., Tang, H., Zhang, Z., Wang, J., and Cao, S., “A retarding potential analyzer design for keV-level ion thruster beams A retarding potential analyzer design for keV-level ion thruster beams,” *Review of Scientific Instruments*, vol. 87, 2016.

[12] Kipritidis, J., Khachan, J., Fitzgerald, M., and Shrier, O., “Absolute densities of energetic hydrogen ion species in an abnormal hollow cathode discharge,” *Physical Review E - Statistical, Nonlinear, and Soft Matter Physics*, vol. 77, 2008.

[13] Kanarov, V., Siegfried, D., Sferlazzo, P., Hayes, A., and Yevtukhov, R., “High resolution energy analyzer for broad ion beam characterization,” *Review of Scientific Instruments*, vol. 79, 2008.

[14] Knudsen, W. C., “Finite grid radius and thickness effects on retarding potential analyzer measured suprathermal electron density and temperature,” *Journal of Geophysical Research*, vol. 97, 1992.

[15] Kononenko, T. V., Konov, V. I., Garnov, S. V., Klimentov, S. M., and Dausinger, F., “Dynamics of deep short pulse laser drilling: Ablative stages and light propagation,” *Laser Physics*, vol. 11, 2001, pp. 343–351.

[16] Michalowski, A., Freitag, C., Weber, R., and Graf, T., “Laser surface structuring with long depth of focus,” *Laser Applications in Microelectronic and Optoelectronic Manufacturing (LAMOM) XVI*, 79200W, 2011.

[17] Finger, J., and Reininghaus, M., “Effect of pulse to pulse interactions on ultra-short pulse laser drilling of steel with repetition rates up to 10 MHz,” *Optics Express*, vol. 22, 2014.

[18] Weber, R., Graf, T., Freitag, C., Feuer, A., Kononenko, T., and Konov, V. I., “Processing constraints resulting from heat accumulation during pulsed and repetitive laser materials processing,” *Optics Express*, vol. 25, 2017.

[19] Förster, D. J., Weber, R., Holder, D., and Graf, T., “Estimation of the depth limit for percussion drilling with picosecond laser pulses,” *Optics Express*, vol. 26, 2018.

[20] Weber, R., Graf, T., Berger, P., Onuseit, V., Wiedenmann, M., Freitag, C., and Feuer, A., “Heat accumulation during pulsed laser materials processing: erratum,” *Optics Express*, vol. 22, 2014.

[21] Di Niso, F., Gaudiuso, C., Sibillano, T., Mezzapesa, F. P., Ancona, A., and Lugarà, P. M., “Role of heat accumulation on the incubation effect in multi-shot laser ablation of stainless steel at high repetition rates,” *Optics Express*, vol. 22, 2014.